# Solution Behavior of Poly(styrene)-*block*-poly(2-vinylpyridine) Micelles Containing Gold Nanoparticles

**Stefan Mössmer, Joachim P. Spatz, and Martin Möller***

*Organische Chemie III, Makromolekulare Chemie, Universität Ulm, D-89081 Ulm, Germany*

**Thomas Aberle, Jürgen Schmidt, and Walther Burchard**

*Institut für Makromolekulare Chemie, Universität Freiburg, D-79104 Freiburg, Germany*

*Received November 30, 1999; Revised Manuscript Received March 1, 2000*

ABSTRACT: Formation and structural transformation of inverse poly(styrene)-*block*-poly(2-vinylpyridine) micelles whose polyvinylpyridine core was loaded with $HAuCl_4$ or with elementary gold nanoclusters was studied by combined static and dynamic light scattering. A transformation in the morphology from spherical particles (small $R_g/R_h$ ratio) to large anisomeric objects (large $R_g/R_h$ ratio) was observed by decreasing the concentration of the block copolymer below the critical micelle concentration. At this point, the polymer chains are molecularly dispersed and no longer able to prevent uncontrolled growth of the gold nanoclusters.

## Introduction

Amphiphilic diblock copolymers associate to form micelles in solvents that dissolve only one of the blocks well. Above a critical micelle concentration (cmc), unfavorable contacts between the core-forming block at one side and the solvent and corona block on the other side favor the association of diblock copolymer chains against entropic energy penalty, i.e., chain crowding and chain stretching.[1] In the last few years, many experimental and theoretical efforts were directed toward the understanding of the fundamental behavior of diblock copolymer micelles in organic as well as in nonorganic solvents. Critical micelle concentrations of diblock copolymers were investigated by size exclusion chromatography, fluorescence spectroscopy, viscosimetry and scattering methods, like static and dynamic light scattering, X-ray and neutron scattering.[2−7] The absolut value of the cmc and the number of associated chains were shown to be controlled mainly by the molecular weight and the interaction parameter $\chi_{core-solvent}$ and $\chi_{core-shell}$. The concentration of free chains above the cmc was found to depend strongly on the molecular weight and also the molecular weight distribution of the diblock copolymers.[8,9] In most cases, diblock copolymers associate to spherical micelles. Cylindrical or platelike micelles, which are well-known for low molecular weight surfactants, are less likely to be formed with polymers.[10] The cause for this is found in the flexible coiled conformation of macromolecules. As the volume fraction of the core-forming block is increased in comparison to the shell-forming block, the blocks can deform this way, adjusting the interfacial area per molecule and molecular packing in spherical associates. Different morphologies have been reported by A. Eisenberg for poly(styrene)-*block*-poly(acrylic acid) block copolymers forming "crew-cut micelles" (i.e., micelles with a very short corona block) in aqueous solution, i.e., spheres, rods, lamellae, vesicles, and complex aggregates of micelles, only when the outer block became very short.[11−13]

Inverse micelles are formed from poly(styrene)-*block*-poly(2-vinylpyridine) diblock copolymers in toluene, i.e., a shell of PS and a polar core of P2VP chains. The incompatibility between the core and the solvent/shell phase ($\chi_{core-solvent}$; $\chi_{core-shell}$) can be enhanced by partially neutralizing the 2VP monomer units of the core-forming block by tetrachloroauric acid.[14] To minimize the unfavorable contacts, the core chains stretch and the number of associated chains per micelle is increased, which minimizes the overall enthalpic interaction. In the case of a short outer block, i.e., a "crew cut micelle", spherical micelles are formed at dilute solutions. However, upon evaporation of the solvent cylindrical micelles with an aspect ratio up to 10.000 were observed.[15]

This structural transformation of the PS-*b*-P(2VP$H^+$-$AuCl_4^-$) micelles is of interest concerning the fundamental structure−property relationships of diblock copolymer micelles. Furthermore, we employ such micelles as a nanoscopic reaction vessel to grow nanocrystals of defined size[16] and to arrange them in highly ordered pattern.[17] Cylindrical micelles offer a route to line pattern, and if the inorganic component is a metal such as gold, it might be possible to obtain nanowires. Yet our ability to control the transformation of the spherical to cylindrical micelles is poorly developed, and we need to develop a more detailed insight in the structure and stability regimes of the associates. This includes the effect of additives which are selectively taken up in the core of the micelles such as the inorganic salt, and the reagents that are added effect the transformation of the former to a nanoparticle.

This work describes the solution behavior of poly(styrene)-*block*-poly(2-vinylpyridine) diblock copolymers (PS-*b*-P2VP) in toluene modified by the addition of $HAuCl_4$ and $N_2H_4$. Investigations have been done including transmission electron microscopy (TEM) and static and dynamic light scattering (SLS, DLS). Tetrachloroauric acid is selectively taken up by the poly(2-vinylpyridine) core of the block copolymer micelles due to the protonation of the pyridine units. Because of its polarity, $N_2H_4$ is also solubilized preferentially in the core of the micelles, where it induces the reduction and

* To whom correspondence should be sent

10.1021/ma992006i CCC: $19.00 
Published on Web 06/02/2000

**Table 1. Molar Amounts of Tetrachloroauric Acid and Hydrazine**

| polymer[a] | $m$ (polymer) [mg] | $V$ (toluene) [mL] | $L$ [$Au^{3+}$/2-VP] | $n$ ($Au^{3+}$) [$\times 10^{-5}$ mol] | $n$ ($N_2H_4$) [$\times 10^{-5}$ mol] | $V$ ($N_2H_4$)[b] [$\mu$L] |
|---|---|---|---|---|---|---|
| PS(300)-*b*-P2VP(300) | 12.5 | 2.5 | 0.5 | 2.99 | 2.24 | 7.0 |
| PS(325)-*b*-P2VP(75) | 12.5 | 2.5 | 0.5 | 1.12 | 0.84 | 2.64 |

[a] Numbers in brackets refer to the degree of polymerization of the PS and the P2VP blocks, respectively. [b] 10 times the amount of anhydrous hydrazine than stoichiometrically needed.

precipitation of the gold. HCl can be added as a scavenger for excess hydrazine which is thus precipitated as hydrazinium chloride.

## Experimental Section

PS-*b*-P2VP block copolymers with different block lengths were synthesized by living anionic polymerization.[17,18] A 0.5 wt % solution of the block copolymer in dry toluene was mixed with 0.5 equiv of $HAuCl_4 \cdot 3H_2O$ per pyridine unit. The mixture was stirred for at least 24 h to allow complete solubilization of the gold acid in the cores of the block copolymer micelles. An aliquot of this solution (2.5 mL) was added to 5 mL of toluene containing a 10-fold stoichiometric excess of anhydrous hydrazine with respect to the gold acid. Anhydrous hydrazine was prepared by thermolysis of hydrazine cyanurate at a high vacuum line and stored in a glovebox under nitrogen.[17]Aqueous HCl (38%) was added to the solution after reduction. Hydrazinium chloride ($N_2H_5Cl$) precipitated and was removed by centrifugation. Thin films were prepared either by dipping[19] or by putting a drop of the solution onto a carbon-coated copper grid, which was in direct contact with a soaking tissue in order to achieve the immediate formation of a thin liquid film from which the actual coating was formed by drying.

**Bright-field transmission electron microscopy** images were recorded with a PHILIPS EM 400 T microscope operating at 80 kV. To minimize the destruction of the polymer by the electron beam, the electron beam intensity was kept as low as possible (second condenser lens, 50 Pt; objective lens, 30 Au).

**UV−vis absorption spectroscopy** was carried out with a Lambda 16 UV−vis absorption spectrometer from Perkin-Elmer.

**Light scattering measurements** were performed with solutions in the concentration range 0.03−3 mg/mL. Solutions were filtered through PTFE filters of 0.2 $\mu$m or 0.5 $\mu$m pore size (Milex-FGS and Milex-SR, respectively). Cylindrical cuvettes of 8 mm in diameter were used. No absorption correction was applied. A fully automated and computer driven ALV goniometer was used that was equipped with an ALV-5000 correlator (ALV Laser Vertrieb GmbH, Langen, Germany). The corresponding software version 5.0 was applied.[20] A 3 W krypton ion laser (Spectra Physics, type 2020) with a red line of $\lambda = 647$ nm served as the light source. Combined static and dynamic LS measurements could be carried out with this instrument. The scattering intensity was measured in an angular regime from 30 to 150° in steps of 10°.

The radius of gyration was determined from Berry plots of the static LS intensities, and the hydrodynamic radius was obtained by a so-called cumulant fit of the intensity−time correlation functions for determining the translational diffusion coefficient and application of the Stokes−Einstein relationship (see Theoretical Section).

## Theoretical Section

Characterization of simple macromolecules and colloidal particles by light scattering (LS) is now a routine technique, and for evaluation, common textbooks of polymer and colloid science could be consulted. In the present case, however, block copolymers are to be characterized which in addition are markedly colored. Both facts make the evaluation of scattering intensities rather complex and require some comments.

**Static Light Scattering.** For the evaluation of molar masses the value for the contrast factor K has to be known. The contrast between dissolved particles and the solvent depends on the square of the refractive index increment d$n$/d$c$. This quantity is usually measured in special differential refractometers, which contain two compartments. In the one, the solvent is filled in the other the solution of a special concentration, and the difference in the refractive index is directly measured. However, for copolymers often serious errors are introduced by a preferential adsorption to one of the two components. The problem can be circumvented when an equilibrium dialysis is applied and now the difference in the refractive indices between the two dialyzed components is measured. Even more pronounced may be the effect of color, because now some quantum mechanical effects may be involved which so far have not yet been studied quantitatively.

Because of these uncertainties we did not consider the absolute scattering intensities and did not determine the molar mass of the particle. Instead, we confined ourselves to the evaluation of the angular envelope of the scattering intensities. The angular dependence is usually normalized by the scattering intensity at zero scattering angle and is called particle scattering (or particle structure) factor $P(q)$

$$P(q) \equiv \frac{i(q)}{i(q=0)} \tag{1}$$

where $q = (4\pi n_0/\lambda)\sin(\theta/2)$ is the magnitude of the scattering vector with $\theta$ the scattering angle and $n_0$ the refractive index of the solvent.

The particle scattering factor is a structure-sensitive function, but for sufficiently small scattering angles a linear expansion can be made that is independent of the particle shape. In the Debye-Zimm representation this is

$$\frac{1}{P_z(q)} = 1 + \frac{1}{3}R_g{}^2q^2 - \ldots \tag{2}$$

in which $R_g{}^2$ is the mean square radius of gyration, defined as

$$R_g{}^2 = \frac{1}{m}\int_0^\infty r^2\,\mathrm{d}m = \frac{1}{m}\int_0^\infty \left(\frac{m}{V}\right)r^2\,\mathrm{d}V \tag{3}$$

with $m$ the mass, $V$ the volume of the particle, and $r$ the distance from the center of mass within a particle. For hard spheres the radius of gyration is related to the sphere radius $R$ as

$$R_g = 0.778R \tag{4}$$

Equation 2 represents a good approximation if $qR_g < 1$, and it is independent of the particle architecture.

**Dynamic Light Scattering.** In dynamic LS a time correlation function (TCF) of the scattering intensity is

**Table 2. Values of the Ratio $\rho = R_g/R_h$ for Different Particle Morphologies[22]**

| architecture | $\rho$ | $C$ |
|---|---|---|
| homogeneous sphere | 0.778 | 0 |
| random coil, monodisperse | | 1.50−1.02 |
| hind;1gΘ conditions | 1.50 | 0.173 |
| good solvent | 1.78 | |
| random coil, polydisperse, $z = 1$ | | |
| Θ conditions | 1.73 | 0.200 |
| good solvent | 2.05 | |
| regular stars | | 0.3−0.55 |
| Θ conditions, $f = 4$ | 1.33 | 0.148 |
| Θ conditions, $f \gg 1$ | 1.079 | 0.098 |
| rigid rod | | |
| monodisperse | >2.0 | 0.042 |
| polydisperse, $z = 1$ | >2.0 | 0.16 |

measured that is given as

$$g_2(t,q) = \frac{\langle i(0)i(t)\rangle}{\langle i(0)\rangle^2} \tag{5}$$

in which $i(0)$ and $i(t)$ are the scattering intensities at time $t = 0$ and a certain delay time $t$ later. For sufficiently short delay times ($t \approx 10^{-6}-10^{-3}$ s), the TCF decays exponentially from a value of about 2 to 1 (baseline) at $t \rightarrow \infty$. For uniform hard spheres, the decay is exactly a single exponential and is related to the mutual diffusion coefficient $D$ as

$$g_2(t,q) = 1 + \exp(-2Dq^2t) \tag{6}$$

The mutual diffusion coefficient in general depends on the concentration and approaches the translational diffusion coefficient $D_{trans}$ at $c = 0$. It is related to the hydrodynamically effective radius $R_h$ of the particle via the Stokes−Einstein relationship

$$D_{trans} = \frac{kT}{6\pi\eta_0 R_h} \tag{7}$$

In general the two radii $R_g$ and $R_h$ differ in value. For hard spheres one has

$$R_g = 0.778R_h \tag{8}$$

but the prefactor $\rho \equiv R_g/R_h$ varies for different particle architectures or geometries and is a valuable parameter for structure estimation. The $\rho$ parameter was calculated for various macromolecular architectures[21] and is collected in Table 2.

In general, the $\rho$ value is as larger as less compact and as more anisometric the particles are. The table contains also values for the parameter $C$ to be defined below (see eq 15). The reason for the structure dependence is based on the hydrodynamic interaction among the polymer segments which increases with the internal segment density of a particle. A simple explanation for this effect is given in Figure 1.[22]

The values in Table 2 were calculated on the basis of Kirkwood's preaverage approximation for the hydrodynamic interaction (Oseen tensor).[23] In an experimental test for star branched macromolecules, Huber et al.[24] noticed that all experimental data were 12−25% lower than predicted. A few years later Freire et al.[25] performed Brownian motion simulations avoiding Kirkwood's preaverage approximation. They now found excellent agreement with the experimental data; the results have been recently reviewed.[26] For monodisperse

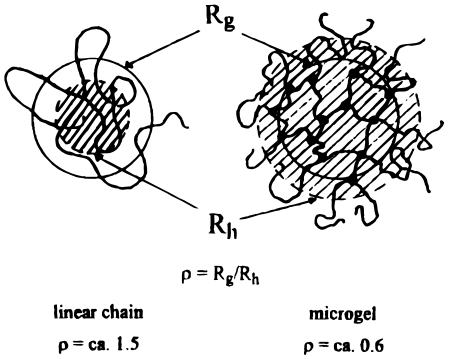


**Figure 1.** Demonstration of the effect of draining on the hydrodynamic radius of particles. The fairly open structure of a flexible linear chain is compared with that for a microgel having the same radius of gyration (full lines). Because of its high segment density the microgel is drained only at its periphery (large $R_h$), whereas the solvent can drain the coil far more deeply (low $R_h$). Reproduced with permission from ref 22. Copyright Clarendon Press 1996.

rods the $\rho$ parameter is given approximately by[27a]

$$\rho \approx (L/d)\ln(L/d - 0.5) \tag{9}$$

Much larger values are obtained for polydisperse rods and values up to 5.5 can be realized even for aspect ratios $L/d < 20$. (See ref 27a and appendix of ref 27b.) Although the values in Table 2 are not absolutely correct, they still give the right tendency and can be used for an estimation of structures.

In most cases, the intensity TCF is not a single exponential. The deviations result from nonuniformity and, for soft particles, from internal modes of motion. The evaluation of the TCF now becomes more complex. As a first step it is necessary to step down to the electric field correlation function that is given by

$$g_1(t,q) = \frac{S(q,t)}{S(q)} = \frac{|\langle E^*(0)\, E(t)\rangle|}{\langle E^*(0)\, E(0)\rangle} \tag{10}$$

In this equation $S(q)$ and $S(q,t)$ are the static and dynamic structure factors, $E(t)$ is the scattered electric field at time $t$ and $E^*(0)$ the conjugated complex quantity at zero time. The two TCFs are correlated to each other, and this sometime in a rather complex manner, but for dilute solutions usually the Siegert relationship holds true which is

$$g_2(t,q) = 1 + [g_1(t,q)]^2 \tag{11}$$

The field TCF $g_1(t,q)$ is accessible to theoretical model calculations and derivations have been successful in some special cases. For unknown structures, the TCF can be approximated by a cumulant expansion that is given as

$$\ln g_1(t,q) = -\Gamma_1(q)t + \frac{\Gamma_2(q)}{2!}t^2 - \frac{\Gamma_3(q)}{3!}t^3 + \ldots \tag{12}$$

in which the $\Gamma_i$ ($i = 1, 2, 3, \ldots$) are the $i$th cumulant of the TCF. Of special interest is the first cumulant, for which one has

$$\Gamma_1(q) = q^2D_z \tag{13}$$

in which the index $z$ indicates the $z$-average of the mutual diffusion coefficient over the whole ensemble of

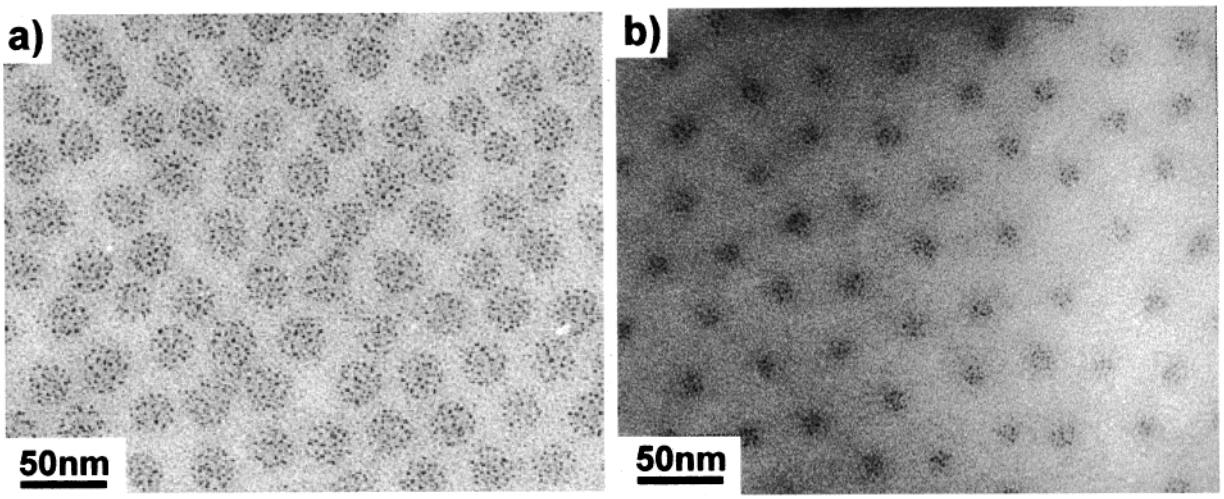


**Figure 2.** Transmission electron micrographs of (a) a monofilm of dried PS(300)-*b*-P[2VP($HAuCl_4$)$_{0.5}$(300)] and (b) of PS(325)-*b*-P[2VP($HAuCl_4$)$_{0.5}$(75)] block copolymer micelles, cast from solution on a carbon-coated copper grid.

particles. Application of the Stokes−Einstein relationship shows that the hydrodynamic radius is actually defined through the *z*-average of the reciprocal hydrodynamic radius of the individual particles

$$\frac{1}{R_h} \equiv \left\langle \frac{1}{R_{h,\text{indiv. particles}}} \right\rangle_z \qquad (14)$$

For flexible particles, eq 13 becomes even more complex because $\Gamma_1(q)/q^2 \equiv D_{app}(q)$ is often angular dependent, and an extrapolation of the apparent diffusion coefficient to zero scattering angle is required before the hydrodynamic radius can be calculated. In a first approximation the angular dependence is given by the equation[21]

$$\frac{\Gamma_1(q)}{q^2} \equiv D_{app}(q) = D_z(1 + CR_g^2q^2 - ...) \qquad (15)$$

The coefficient $C$ is determined by the slowest internal mode of motion, e.g., the rotational diffusion coefficient for rodlike structures[27a] or the "breathing" mode in flexible coils. The theoretical values for various structures are collected in Table 2. For monodisperse rigid rods the $C$ parameter is zero. Polydispersity however shifts both the $\rho$ and $C$ parameters to higher values, and a weak angular dependence is now observed also for rigid spheres.

## Results and Discussion

PS-*b*-P2VP diblock copolymers were dissolved in toluene at a concentration of $c = 5$ mg/mL. A stoichiometric equivalent of tetrachloroauric acid was added to the micellar solution, i.e., $HAuCl_4$/2-VP = 0.5. Protonation of the 2-VP units resulted in the formation of a polyionic block.

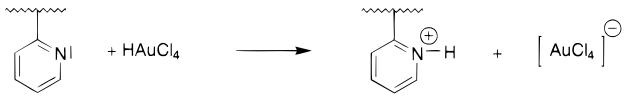


A closed monofilm of the micelles was prepared either by dipping a suitable substrate, e.g., a carbon-coated copper grid, or by putting a drop of the dilute solution onto the substrate. Figure 2 shows TEM micrographs of such monofilms: (a) PS(300)-*b*-P[2VP($HAuCl_4$)$_{0.5}$(300)] and (b) PS(325)-*b*-P[2VP($HAuCl_4$)$_{0.5}$(75)] diblock copolymer micelles cast on a carbon-coated copper grid from a solution of $c = 1$ mg/mL (numbers in brackets refer to the number of repeating monomer units).

The core of each micelle is marked by many ultrasmall Au particles. They were formed because the electron irradiation effects instantaneous reduction of the gold salt.

$$2HAuCl_4 + 6e^- \rightarrow 2Au + 2HCl + 3Cl_2$$

The center to center distance of the hexagonally arranged micelles is controlled by the shell of PS, which is not visible in the TEM because of its small electron density. One gold particle in each diblock copolymer micelle was obtained when 2.5 mL of a $c = 5$ mg/mL solution were treated with a 10-fold excess of anhydrous hydrazine, which itself was dissolved in toluene to 0.1 vol %. Because of its polar character, hydrazine is taken up preferentially in the core of the micelles where it reduces $Au^{3+}$ to $Au^0$.

$$4HAuCl_4 + 3N_2H_4 \rightarrow 4Au + 3N_2 + 16\ HCl$$

The originally colorless solution turned first bluish and then deep purple within a few seconds. Figure 3 a shows a TEM micrograph of a monofilm of PS-*b*-P2VP/Au micelles that was prepared by casting a drop of the purple $c = 1$ mg/mL solution onto a carbon-coated copper grid directly after reduction.

The black spots represent gold particles of 9 nm diameter. The uniform particle to particle distance of 30 nm is controlled by the polymeric shell. When a smaller amount of anhydrous hydrazine was added, an increase in the particle size distribution was obtained, indicating that the particle formation did not occur in all micelles simultaneously. A 10-fold excess of the reducing agent was the minimum amount necessary to form exactly one gold particle in each micelle. Neutralization of the excess $N_2H_4$ with HCl and precipitation of $N_2H_5Cl$ is essential for long-term stability of the colloidal dispersion with single gold particles in each micelle. The excess of $N_2H_4$ was removed directly after reduction by adding 15 $\mu$L of 38% aqueous HCl.

$$N_2H_4 + HCl \rightarrow N_2H_5Cl$$

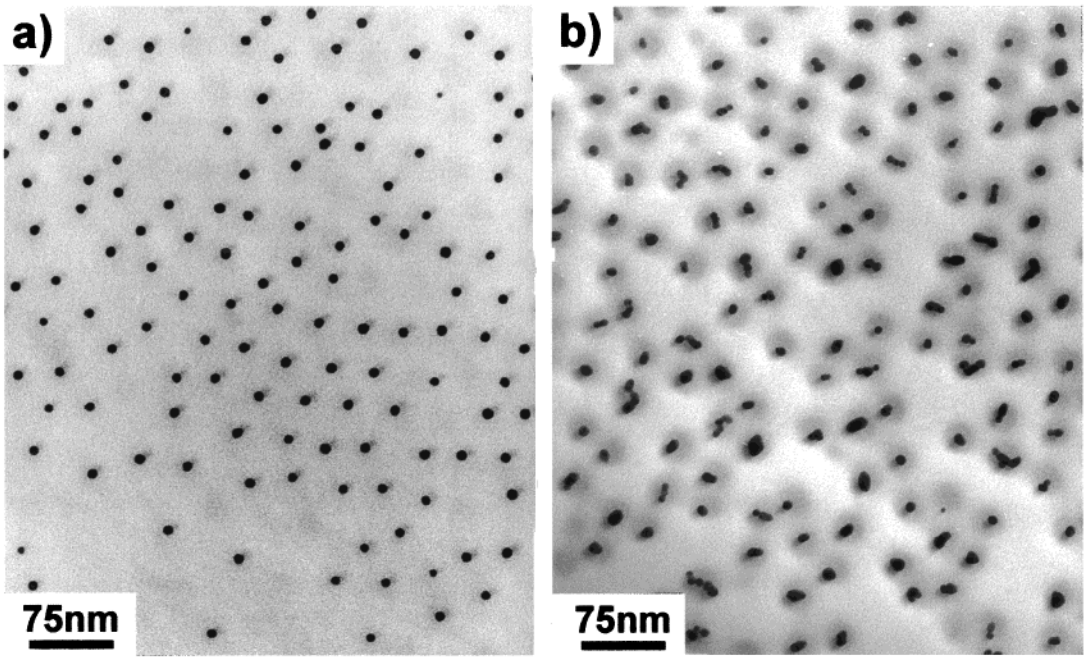


**Figure 3.** TEM images of dried films of block copolymer micelles in which $HAuCl_4$ was transformed to a small gold particle. Key: (a) 9 nm isolated gold particles cast from solution of PS(300)-*b*-P[2VP·$Au_{0.5}$(300)] directly after reduction; (b) Micelles containing two to four gold particles, cast from a solution of PS(300)-*b*-P[2VP·$Au_{0.5}$(300)] 30 min after reduction.

The precipitated hydrazinium chloride was finally removed by centrifugation. This way it was possible to stabilize the purple solution in such a way that identical TEM images were obtained from monofilms which were cast many days later. Figure 3b shows a TEM micrograph of a film which was cast from a solution which was not treated by HCl but aged for about 15−20 min after addition of hydrazine. During this time, the color of the solution had changed again from purple to blue. The micrograph demonstrates that gold particles of equal size are coagulated to groups of two to four particles. This agglomeration of the gold particles can be explained by coagulation of two to four micelles. As the excess $N_2H_4$ swells the core volume, the block copolymer chains are not sufficient for stabilizing the core interface anymore. Two, sometimes three micelles coagulate forming a miniemulsion droplet.

Because of the change in color, coagulation of the micelles and the agglomeration of the gold particles can be followed in solution by UV−vis spectroscopy.[28] Figure 4 shows UV−vis spectra of different micellar solutions ($c$ = 0.3 mg/mL in all cases):

After addition of the reducing agent, the originally yellowish colored solution, spectrum a, changed immediately to a deep purple-red color, spectrum b, while the absorbance of the $PyH^+AuCl_4^-$ ions vanished almost instantaneously. The absorption band at 525 nm is characteristic for the surface plasmon resonance of small Au nanocrystals.[29]

When no HCl was added to the reduced solution, the bluish color developed after half an hour, characterized by spectrum c in Figure 4. The shoulder at higher wavelength is explained by the close proximity of the paired particles. Depending on the polarization of the electric field with respect to the axis between the adjacent gold particles, electromagnetic coupling of the dipole oscillations occurs, originally described by Mie.[29]

Dynamic light scattering (DLS) was applied to determine the hydrodynamic radius $R_h$ of the micelles in the different solutions. Figure 5 shows $R_h$ plotted vs the

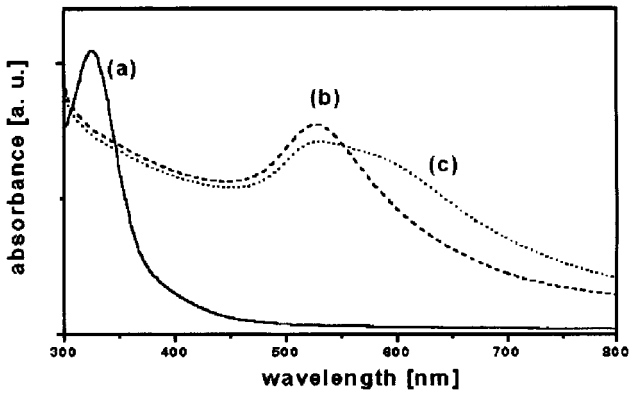


**Figure 4.** UV−vis absorbance spectra of a solution of PS(300)-*b*-P[2VP($HAuCl_4$)$_{0.5}$(300)]: (a) before addition of the reducing agent; (b) directly after reduction with anhydrous hydrazine; (c) after an additional 30 min.

concentration for the micelles of PS(300)-*b*-P[2-VP($HAuCl_4$)$_{0.5}$(300)]. The three examples were (i) micelles loaded with the gold salt, (ii) a purple red solution of micelles which contained one gold particle each and (iii) a bluish solution with micelles containing two to four gold particles each. In all cases, $R_h$ was constant from 0.3 to 2.0 mg/mL. Measurements at higher concentrations were influenced by strong absorption or multiple scattering, and no reliable data could be determined.

The hydrodynamic radius of the micelles loaded with $HAuCl_4$ was observed to be 28 nm. After reduction and in the case where excess hydrazine was scavenged by addition of HCl, $R_h$ was measured to be 30 nm for the micelles containing one gold particle each. When the micellar solution was not stabilized immediately and the $N_2H_4$ swollen micelles coagulated mostly pairwise before addition of HCl, $R_h$ increased to 38 nm. The increase from 28 to 30 nm is explained by incorporation of some $N_2H_4$/HCl in the micellar core. The further increase to 38 nm by coagulation of the nonstabilized micelles is in good agreement with the average periodicities in the TEM images, shown in Figure 3.

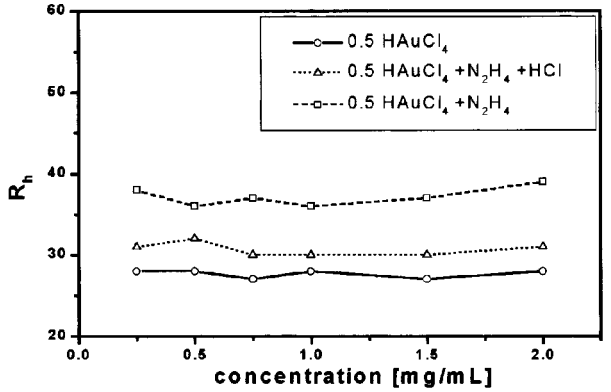


**Figure 5.** Plot of the hydrodynamic radius $R_h$ vs the concentration ($c = 0.25-2.0$ mg/mL) for gold-loaded PS(300)-*b*-P2VP(300) micelles in toluene: (○) PS(300)-*b*-P[2-VP(HAuCl$_4$)$_{0.5}$(300)]; (△) PS(300)-*b*-P[2-VP(HAuCl$_4$)$_{0.5}$(300)] after $N_2H_4$ treatment yielding one gold particle in each micelle; (□) PS(300)-*b*-P[2-VP(HAuCl$_4$)$_{0.5}$(300)] after hydrazine reduction yielding two gold particles in each micelle.

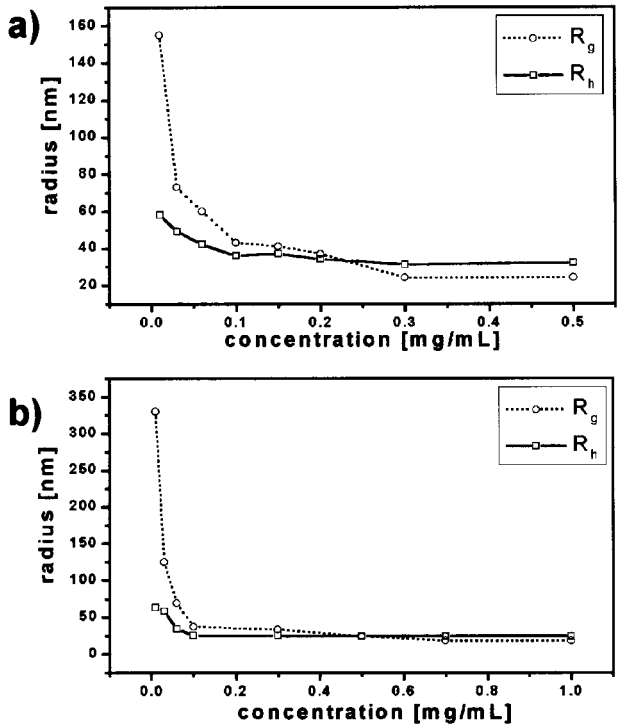


**Figure 6.** Plot of $R_h$ and $R_g$ of stabilized gold particles within one block copolymer micelle vs the concentration: (a) PS(300)-*b*-P[2VP·Au$_{0.5}$(300)] and (b) PS(325)-*b*-P[2VP·Au$_{0.5}$(75)]) (○, $R_g$; □, $R_h$).

The scattering experiments described so far were conducted well above the critical micelle concentration.[14] Parts a and b of Figure 6 show the concentration dependence of $R_h$ and $R_g$ ($R_g$ from static LS) for micellar solutions with one gold particle per micelle including concentrations smaller than 0.3 mg/mL. Because of the gold particles, the refractive index increment d*n*/d*c* could not be determined and consequently no weight-average of the molecular weight was evaluated. Two different block copolymers were employed, i.e., one with a long and one with a short poly(2-vinylpyridine) block. The samples were prepared in a manner identical with the ones described above and diluted to low concentrations. First the block copolymer was dissolved at a rather high concentration ($c = 5$ mg/mL) loaded with 0.5 equiv of $HAuCl_4$ per micelle. The $Au^{3+}$ was reduced by $N_2H_4$. The excess of $N_2H_4$ was precipitated by the addition of HCl·aq and the supernatant solution was diluted further.

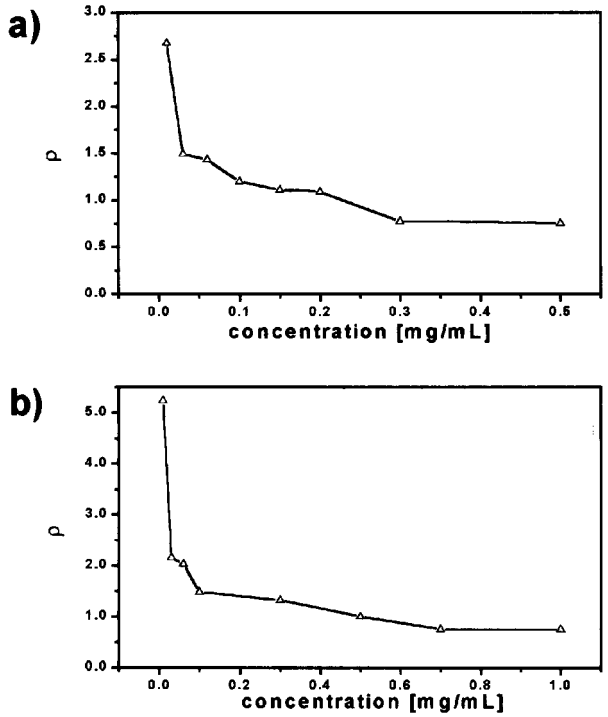


**Figure 7.** Plot of $\rho$ vs the concentration for block copolymer stabilized gold particles: (a) PS(300)-*b*-P[2VP·Au$_{0.5}$(300)] and (b) PS(325)-*b*-P[2VP·Au$_{0.5}$(75)].

**Table 3. $\rho$ Values in Dependence on the Concentration for Two Different Polymeric Systems**

| PS(300)-*b*-P[2VP·Au$_{0.5}$(300)] | | PS(325)-*b*-P[2VP·Au$_{0.5}$(75) | |
|---|---|---|---|
| concn [mg/mL] | $\rho$ [$R_g/R_h$] | concn [mg/mL] | $\rho$ [$R_g/R_h$] |
| 0.5 | 0.75 | 1.0 | 0.75 |
| 0.3 | 0.77 | 0.7 | 0.75 |
| 0.2 | 1.08 | 0.5 | 1.0 |
| 0.15 | 1.11 | 0.3 | 1.32 |
| 0.1 | 1.19 | 0.1 | 1.48 |
| 0.06 | 1.42 | 0.06 | 2.03 |
| 0.03 | 1.49 | 0.03 | 2.16 |
| 0.01 | 2.67 | 0.01 | 5.24 |

For both polymers, $R_h$ increased with decreasing concentration from 30 to around 50 nm for concentrations smaller than 0.1 mg/mL. Above 0.1 mg/mL, the radii of gyration obtained from static light scattering did not depend on the concentration. However, below 0.1 mg/mL, $R_g$ increased to values up to 160 and 325 nm, respectively. Correspondingly the $\rho$ parameter ($\rho = R_g/R_h$) that is characteristic for the particle shape in solution[21,22] increased strongly at low concentrations for PS(300)-*b*-P2VP(300)- and PS(325)-*b*-P2VP(75) block copolymer micelles, loaded by a gold particle (parts a and b of Figure 7.

Table 3 summarizes the $\rho$ values of stabilized gold particles for the two investigated polymer systems in dependence of the concentration.

In the case of the block copolymer solutions with the gold particles enclosed in the micelles, $\rho$ is close to 0.7 for concentrations larger than 0.3 and 0.6 mg/mL for the PS(300)-*b*-P2VP(300) and the PS(325)-*b*-P2VP(75) block copolymer, respectively. This value is consistent with a globular structure of the micelles. Upon decreasing concentration, the $\rho$ parameter increased to values of around 1.5. Such a $\rho$ parameter is typical for a much less dense particle structure like a star molecule or a

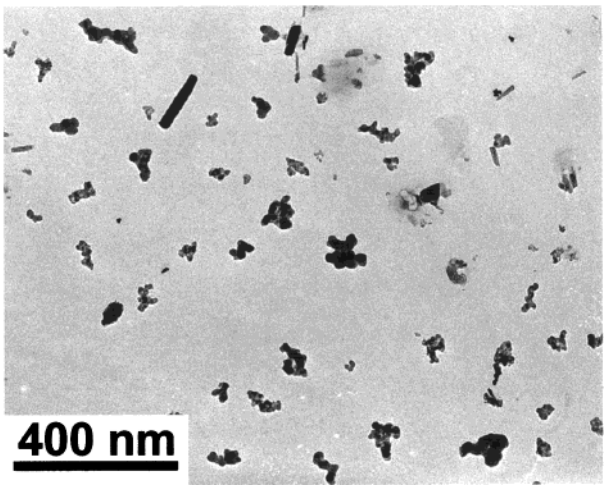


**Figure 8.** TEM image of a dried film of PS(300)-*b*−P[2VP·$Au_{0.5}$(300)], cast from a $c = 0.01$ mg/mL solution on a carbon-coated copper grid.

random coil conformation.[21,24−26] When the concentration was reduced further below 0.05 mg/mL, the $\rho$ value increased sharply. Values higher than 2.2 were observed (2.67 and 5.24, respectively), being typical for non-spherical scattering objects such as rods or elongated spezies.[22,27] Such large $\rho$ parameters cannot be realized by monodisperse rods with an aspect ratio of $L/d < 100$. However, the $\rho$ parameter of elongated structures strongly depends on polydispersity, and values of up to 5.5 can be realized even for $L/d < 20$. Inspection of the transmission electron micrograph (Figure 8) clearly shows the high polydispersity. The unexpected increase in the $\rho$ values can be explained by a loss of control on the particle formation. This became evident when thin films were cast from the very diluted solution and studied by TEM. Figure 8 depicts a transmission electron micrograph of a film cast from a $c = 0.01$ mg/mL solution of PS(300)-*b*-P[2VP·$Au_{0.5}$(300)], which was treated with HCl(aq) after reduction of the gold salt by excess $N_2H_4$.

Agglomerates of gold particles, most of which are non spherical in shape are observed. The formation of anisometric particles is consistent with the increase in $R_g$ and of the $\rho$ parameter (see Table 2). It can be explained by dissolution of the micelles at very low concentrations. Thus, the single particles are not stabilized efficiently and agglomeration can take place. It can be concluded, that the concentration at which the $R_g$ and $R_h$ start to increase and to deviate from each other corresponds to the cmc of the block copolymer, i.e., cmc $\approx$ 0.1 mg/mL. Dissolution of the micelles at low concentrations is consistent with the observation that the steep increase of the $\rho$ parameter occurred in the case of the block copolymer with the shorter P2VP block at higher concentrations than in the case of PS(300)-*b*-P2VP(300) block copolymer. The longer the core-forming block, the lower the cmc of the resulting micelles, if the length of the corona-forming block is approximately the same.[30]

From Figure 7, the cmc of the PS(325)-*b*-P[2VP·$Au_{0.5}$-(75)] and the PS(300)-*b*-P[2VP·$Au_{0.5}$(300)] can be estimated to be $\leq$0.1 and $\leq$0.06 mg/mL, respectively. Below this concentrations, the gold particles coalesce and form the anisotropical scattering objects, which explain the increase in $R_h$ and $R_g$.

## Conclusions

Combination of transmission electron microscopy on dried films of poly(styrene)-*block*-poly(2-vinylpyridine) block copolymer micelles with light-scattering studies on the dilute solutions in toluene yielded a rather detailed insight into the association behavior and the stability of the micelles. Light scattering allowed us to evaluate the critical concentration for the micelle formation and indicated the increase in size as the core of the micelles was swollen by $N_2H_4$. Furthermore, the light-scattering experiments allowed to follow the agglomeration of the gold particles that were originally stabilized by the micellar coat, when the micelles fell apart at decreasing concentration.

**Acknowledgment.** This work was supported by the BMBF (03D0054), the Fond der Chemischen Industrie, and the Deutsche Forschungsgemeinschaft (Pr. Nr. 32 836).

## References and Notes

(1) Tuzar, Z.; Kratochvil, P. *Surface and Colloid Science*; Plenum Press: New York, 1993; Volume 15.
(2) Calderara, F.; Hruska, Z.; Hurtrez, G.; Lerch, J.-P.; Nugay, T.; Riess, G.; *Macromolecules* **1994**, *27*, 1210.
(3) Antonietti, M.; Heinz, S.; Schmidt, M.; Rosenauer, C. *Macromolecules* **1994**, *27*, 3276.
(4) Nguyen, D.; Williams, C. E.; Eisenberg, A. *Macromolecules* **1994**, *27*, 5090.
(5) Khougaz, K.; Astafieva, J.; Eisenberg, A. *Macromolecules* **1995**, *28*, 6055.
(6) Hickl, P.; Ballauf, M.; Jada, A. *Macromolecules* **1996**, *29*, 4006.
(7) Calderara, F.; Riess, G. *Macromol. Chem. Phys.* **1996**, *197*, 2115.
(8) Gao, Z.; Eisenberg, A. *Macromolecules* **1993**, *26*, 7353.
(9) Khougaz, K.; Gao, Z.; Eisenberg, A. *Macromolecules* **1994**, *27*, 6341.
(10) de Gennes, P. G. *Solid State Physics*; Liebert, L., Ed.; Academic Press: New York. 1978; Supplement 14, p 1.
(11) Gao, Z.; Varshney, S.; Wong, S.; Eisenberg, A. *Macromolecules* **1994**, *27*, 7923.
(12) Zhang, L.; Eisenberg, A. *Science* **1995**, *268*, 1729.
(13) Zhang, L.; Eisenberg, A. *J. Am. Chem. Soc.* **1996**, *118*, 3168.
(14) Spatz, J. P.; Sheiko, S.; Möller, M. *Macromolecules* **1996**, *29*, 3220.
(15) Spatz, J. P.; Mössmer, S.; Möller, M.; *Angew. Chem., Int. Ed. Engl.* **1996**, *35*, 1510.
(16) (a) Spatz, J. P.; Mössmer, S.; Möller, M. *Chem.—Eur. J.* **1996**, *2*, 1552. (b) Möller, M.; Spatz, J. P.; Roescher, A.; Mössmer, S.; Tamil Selvan, S.; Klok, H. A. *Macromol. Symp.* **1997**, *117*, 7.
(17) Spatz, J. P.; Mössmer, S.; Hartmann, C.; Möller, M.; Herzog, T.; Krieger, M.; Boyen, H.-G.; Ziemann, P.; Kabius, B. *Langmuir* **2000**, *16*, 407.
(18) (a) Künstle, H. Block Copolymer Composites with Semiconductor Nanocrystals. Ph.D. Thesis, University of Twente, The Netherlands, 1993. (b) Mössmer, S. Size Control of Metallic Nanoparticles and Surface Patterning by Self-Assembly of Diblock Copolymers. Ph.D. Thesis, University of Ulm, Germany, 1999.
(19) Spatz, J. P.; Herzog, T.; Mössmer, S.; Ziemann, P.; Möller, M. *Adv. Mater.* **1999**, *11*, 149.
(20) Bantle, S.; Schmidt, M.; Burchard, W. *Macromolecules* **1982**, *15*, 1604.
(21) (a) Burchard, W.; Schmidt, M.; Stockmayer, W. H. *Macromolecules* **1980**, *13*, 1265. (b) Burchard, W. *Adv. Polym. Sci.* **1983**, *48*, 1.
(22) Burchard, W. Combined Static and Dynamic Light Scattering. In Brown, W., Ed.; *Light Scattering: Principle and Development*; Clarendon Press: Oxford, England, 1996; p 450 ff.
(23) Kirkwood, J. G.; Riseman, J. *J. Chem. Phys.* **1948**, *16*, 565.
(24) Huber, K.; Burchard, W.; Fetters, L. J. *Macromolecules* **1984**, *17*, 54.

(25) (a) Freire, J. J.; Pla, J.; Rey, A.; Prats, R. *Macromolecules* **1986**, *19*, 452. (b) Freire, J. J.; Rey, A.; Garcia de la Torre, J. *Macromolecules* **1986**, *19*, 457. (c) Rey, A.; Freire, J. J.; Garcia de la Torre, J. *Macromolecules* **1987**, *20*, 342.
(26) Burchard, W. *Adv. Polym. Sci.* **1999**, *143*, 111.
(27) (a) Schmidt, M. *Macromolecules* **1984**, *17*, 553. (b) Müller, A.; Burchard, W. *Colloid Polym. Sci.* **1995**, *273*, 866.
(28) Kreibig, U.; Vollmer, M. *Optical Properties of Metal Clusters*; Springer: Heidelberg, 1995.
(29) Mie, G. *Ann. Phys.* **1908**, *25*, 377.
(30) Munch, M. R.; Gast, A. P. *Macromolecules* **1988**, *21*, 1360.

MA992006I